

# ME 7080 - Multidisciplinary Structural Optimization

Final Project: Hypersonic Aircraft Panel Optimization

---

Daniel Clark

May 1, 2015

## ABSTRACT

Hypersonic aircraft provide the strategic potential to perform an aerospace mission anywhere in the world within one hour, the United States Air Force has invested considerable efforts to develop and demonstrate effectiveness of hypersonic technologies. From a structural science and technology perspective, fatigue and creep predictions under the repetitive thermo-mechanical-acoustic loadings from the extreme harsh flight conditions are essential to assess flight critical damage state with high confidence. In this paper, a single cell of a hypothetical hypersonic aircraft's wing-box is optimized utilizing Dassault Systems' Abaqus finite element software, driven by MathWorks' MATLAB technical computing language. Before performing optimization the design space was thoroughly explored utilizing numerous Design of Experiments (D.O.E.s) to prevent any runtime errors. Numerous optimization techniques were utilized including: finite difference convergence studies, function approximations, surrogate modeling (Kriging), surrogate optimization, and gradient based optimization.

## SCOPE OF WORK

Ever since Wilbur and Orville Wright made the first powered aircraft flight on December 17, 1903, the challenge to increase the reliability and performance of air vehicles has pushed industry and researches towards the pursuit of more advanced air vehicles. More than 100 years later, the subsonic, transonic, and supersonic flight regimes have been adequately studied. All of which have or had military and commercial manned air crafts operate within the regime safely. However, the hypersonic regime, mach 5.0-10.0 has had zero declassified manned aircraft and only a handful of unmanned experimental crafts which were able to operate within the regime successfully. Incorporation of more accurate high temperature physics is necessary to design safe and reliable hypersonic air vehicles. Lockheed Martin Aerospace recently entered a 3 phase project with the Air Force Research Lab with the objective of the current predictive

capabilities for hypersonic structural response and life prediction. Phase I and II have been approved for public release [1] [2]. Lockheed Martin investigated the usage of the DARPA Falcon program developed HTV-3X loft (Figure 1) for its translation into an operational vehicle with the hypothetical cruise profile of 30 minutes at mach 5.2. The HTV-3X loft vehicle geometry was modified to enable the extra fuel required for the targeted 30 minute cruise profile.



Figure 1: DARPA Falcon Program HTV-3X Vehicle.

A panel study was conducted of four vehicle study zones, Figure 2. "The study goal for the Panel 3 design and analysis effort was targeted toward a vehicle region where a combination of high dynamic pressure, thermally induced stress, and material property change cause aero-elastic stability to be of primary concern." [2] Panel 3 will be further investigated and optimized within this report.

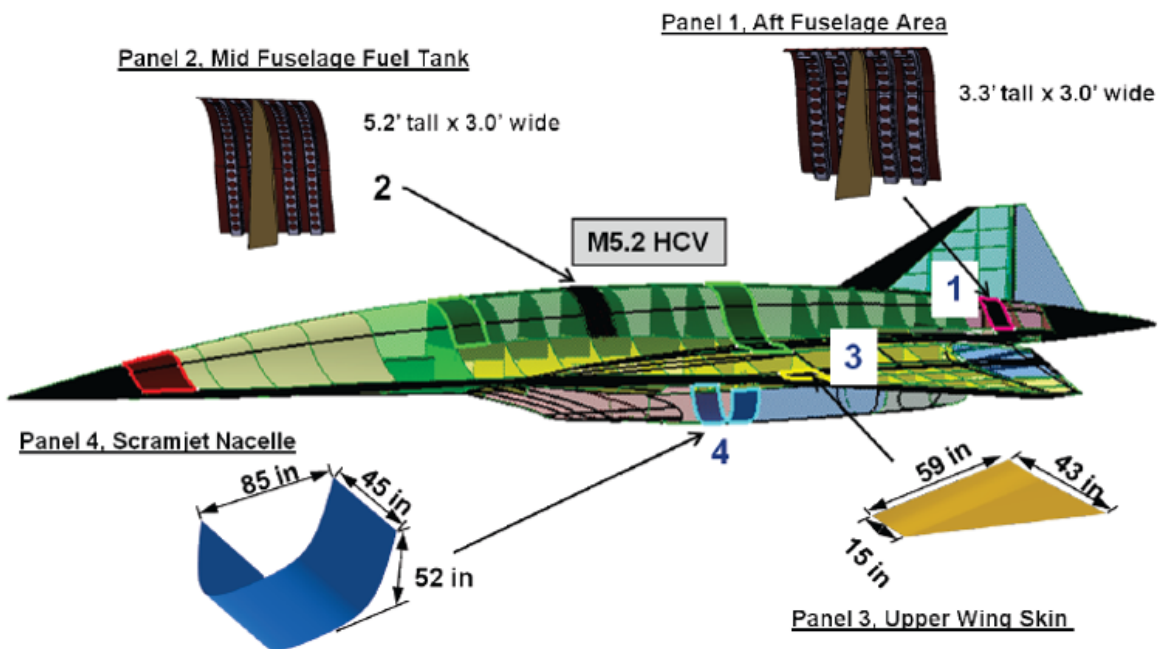


Figure 2: Hypothetical hypersonic aircraft frame with the 4 vehicle study panels labeled respectively.

### PANEL 3 DESCRIPTION

Panel 3, the area just after the wings leading edge experiences high temperature thermal loads coupled with structural and dynamic loads. The current Panel 3 assembly is modeled in Abaqus as 2 sub assemblies. The first sub-assembly includes the top-skin, core and bottom-skin held together with an L shaped frame via "tie" constraints (Figure 3). The core is modeled with solid elements, while the top-skin, frame, and bottom-skin are modeled with shell elements.

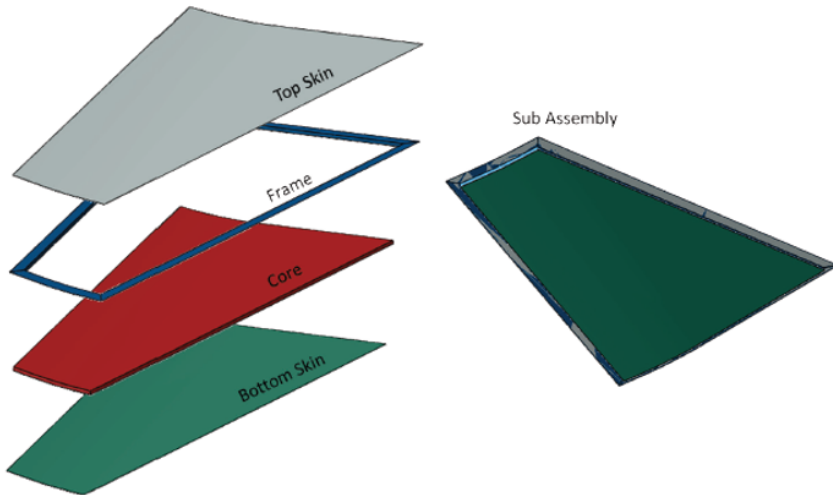


Figure 3: Panel 3B sub assembly: top-skin, frame, core, and bottom-skin.

The first sub-assembly is then added to the second sub-assembly containing the bulkhead (Figure 4). The bulkhead walls were also modeled using shell elements and will not be a primary concern for this study. However, they do contribute to the mass of the structure and act as boundary conditions for the first sub-assembly.

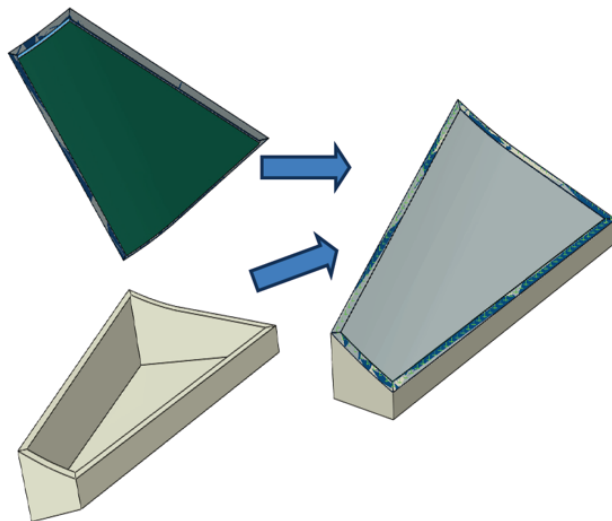


Figure 4: Panel 3B final assembly.

## DESIGN GOALS

The objective of this study is to minimize the mass of the entire assembly (Figure 4) subject to numerous constraints including: maximum principle stress, minimum frequency, minimum displacement, and minimum displacement constraints. Due to the temperature induced stresses the critical zones change depending on the thickness of the components, therefore aggregation strategies are implemented to limit the amount of constraints, these are discussed in detail in the Methodology section. Two different optimization techniques are utilized in this study. The first technique employed is gradient based optimization. In gradient based optimization methods function values and gradients are utilized to move about the design space until the Karush-Kuhn-Tucker conditions are satisfied. These methods can be highly dependent on the

initial conditions but are less costly than global optimization techniques. The specific methods utilized include: interior-point algorithm, sequential quadratic programming and sequential function approximations.

The second technique utilized in this study is surrogate based optimization. In surrogate based optimization a surrogate such as stationary Kriging, is fitted to space filling D.O.E. like Latin Hypercube Sampling (LHS) for all the responses. Then optimized upon with gradient based techniques. The optimal design achieved by the surrogate can then be evaluated using FEA software to check the accuracy of the approximation. This optimal can then be utilized as the starting point of a gradient based optimization algorithm or methods such as Jones's Efficient Global Optimization (EGO) can be employed to update the surrogate until desired accuracy is achieved.

The D.O.E. previously mentioned can also be utilized in design space exploration to ensure that the FEA model behaves properly to the corresponding changes in design variables. In this study, two  $2^k$  factorial design with a center point of different ranges were used to evaluate the stability of the model. Then a LHS design of 200 points was used to construct a stationary ordinary Kriging surrogate to explore the design space.

## METHODOLOGY

Two of the limiting load cases presented in the phase 2 report are utilized in the optimization routine: decent compression size limiting case (M52A LC60076 S02), and cruise tension size limiting case (M20D LC60041 S02). For both cases it is necessary to evaluate the temperatures for both material properties and thermal expansion stresses, therefore the temperature profile case (T01) are ran to evaluate the nodal temperatures at the ascent, cruise and decent stages. Finally, to address the aero-elastic stability of the design, frequency analysis (FREQ) is conducted at a uniform maximum temperature determined by either ascent or cruise. The 4 simulations are all separate Abacus input files ran through the MATLAB command line in interactive mode. The results are interpreted by MATLAB using file input/output operations on the Abaqus \*dat file.

## PROBLEM STATEMENT

The optimization problem statement can be found in Equation 1 in standard form using English units.

$$\begin{aligned}
 \text{Minimize:} \quad & f(\mathbf{x}) = \text{mass} \\
 \text{Subject to:} \quad & g_1(\mathbf{x}) = f - f_{min} \geq 0 \\
 & g_i(\mathbf{x}) = \sigma_1 - \sigma_i \geq 0 \\
 & g_j(\mathbf{x}) = T_{max} - T_j \geq 0 \\
 & g_k(\mathbf{x}) = U_{max} - U_k \geq 0 \\
 \text{Design variables:} \quad & \mathbf{x} = [x_1, x_2, x_3, x_4, x_5, x_6, x_7]^T \\
 \text{Side bounds:} \quad & x_{LB} \leq x_i \leq x_{UB}
 \end{aligned} \tag{1}$$

Where  $x_1$  is the thickness of the top-skin,  $x_2$  is the thickness of the bottom-skin,  $x_3$  is the thickness of the frame,  $x_4$  is the right and left bulkhead walls,  $x_5$  is the front and back bulkhead walls,  $x_6$  is the bottom of the bulkhead,  $x_7$  is the top of the bulkhead,  $f$  is the first natural frequency of the total assembly,  $f_{min}$  is the minimum first natural frequency of the total assembly,  $\sigma_i$  is the max principal stress of different component zones  $i$ ,  $\sigma_1$  is a predefined maximum allowable principal stress,  $T_j$  is the nodal temperature of different component zones  $j$ ,  $T_{max}$  is a

predefined maximum allowable temperature,  $U_k$  is the displacement of different zones  $k$  in the top-skin,  $U_{max}$  is a predefined maximum allowable displacement and  $x_{LB}$  and  $x_{UB}$  are the side bounds for all 7 design variables. For each set of design variables all four of the aforementioned simulations are necessary.

The first simulation is the temperature simulation (T01). T01 uses predefined heat fluxes to determine the temperature the 3 flight stages. The cruise temperature is then imported as the first step of the compression size limiting case and the descent temperature is imported as the first step of the tension limiting case. A simple schematic of the temperature simulation is in Figure 5.

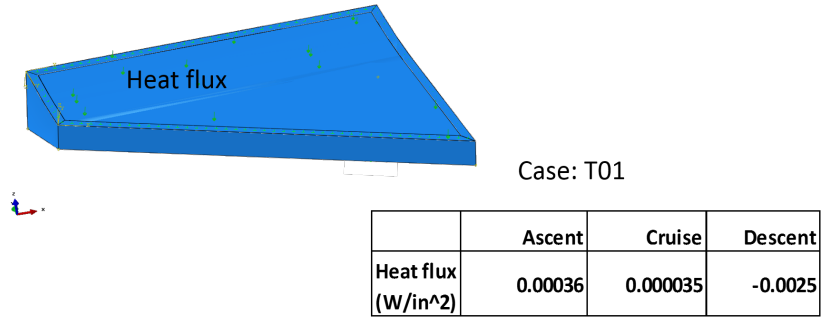


Figure 5: Schematic of temperature simulation with corresponding heat fluxes.

More importantly it is necessary to evaluate the  $g_j$  temperature constraints. Instead of evaluating all of the nodal temperatures, zones of individual components where the maximum values occur are evaluated using an aggregation function. The particular aggregation function utilized is a basic  $p$  – norm measure, Equation 2 demonstrates  $p$  – norm for nodal temperatures.

$$T_{pn} = \left\{ \sum_{node=1}^{N_{node}} \left( \frac{F(T_{node})}{\bar{T}} \right)^p \right\}^{1/p} \quad (2)$$

The  $p$  – norm approximation tends to degrades as the set size is increased therefore it is advantageous to either pick a small set size or a set with similar responses. As,  $P$  tends toward infinity the more the aggregation better approximates the maximum response becoming less differential. The element and node zones for components of interest are below in Figures 6 through 9.

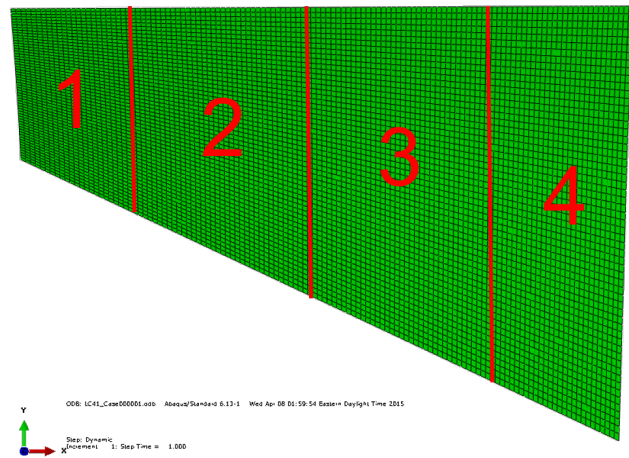


Figure 6: Top-skin element and node zones labeled 1 though 4. Utilized in cases: LC41, LC76 and T01 for nodal temperatures and displacements as well as element principal stresses.

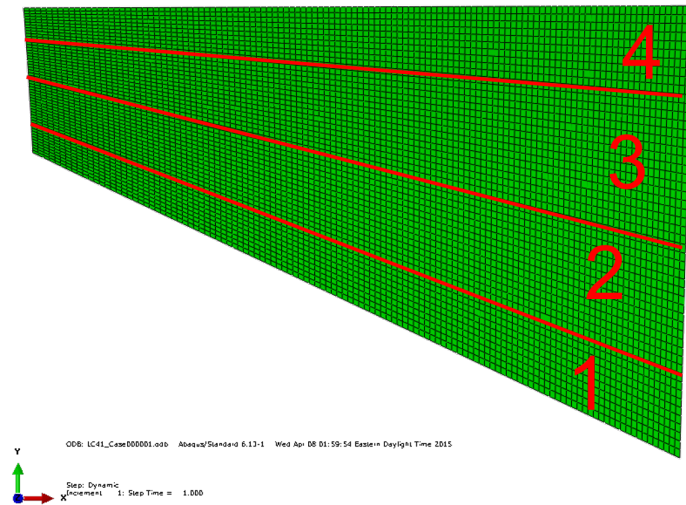


Figure 7: Bottom-skin element zones labeled 1 though 4. Utilized in cases: LC41 and LC76 for element principal stresses.



Figure 8: Frame element zones labeled 1 through 4. Utilized in cases: LC41 and LC76 for element principal stresses.

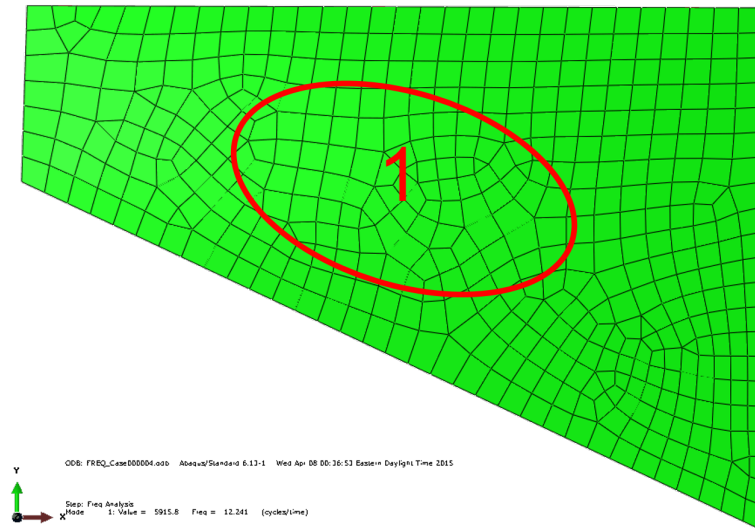


Figure 9: Bottom bulkhead node zone labeled 1. Utilized in case T01 for nodal temperatures.

The aggregation zones are utilized in all of the simulations excluding the frequency analysis since it is the response of the entire system. The third and forth simulations are the compression and tension size limiting cases respectively. The loads and boundary conditions for which are in Figures 10 and 11.

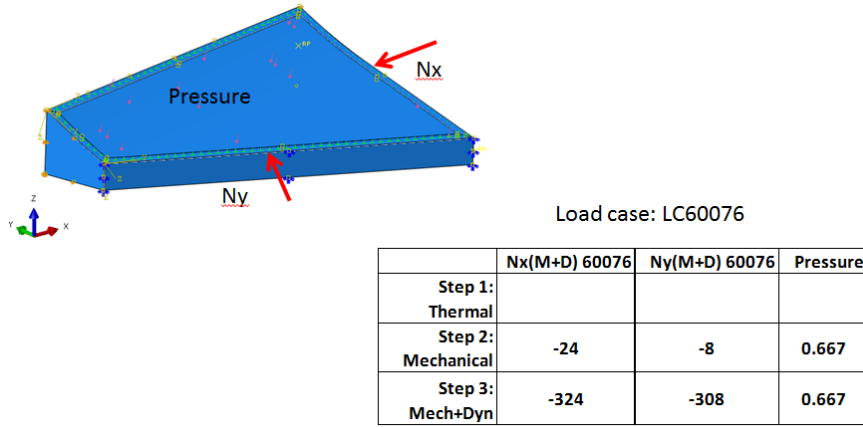


Figure 10: Loading and boundary conditions for the compression sizing case.

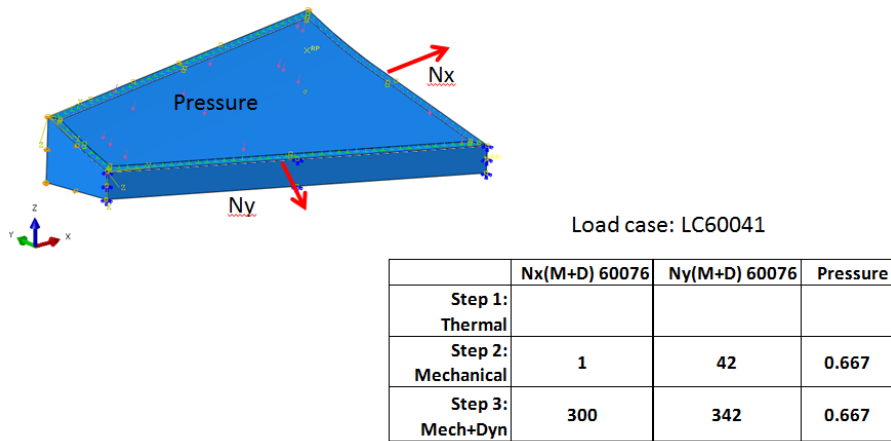


Figure 11: Loading and boundary conditions for the tension sizing case.

To perform the gradient based optimization techniques, gradient information is necessary. Therefore, a finite difference convergence study was conducted to determine the appropriate step size for each variable with respect to each response. This means for every simulation there are 7 additional simulations to determine the gradients using finite difference. The details of the finite difference study are presented and discussed in the following section.

## SOLUTION APPROACH

Before performing optimization the minimum natural frequency, maximum allowable principal stress, maximum allowable temperature, maximum allowable displacement and the design variables side bounds must be defined. The constraint variables were selected based on previous experience. Table 1 outlines the constraint variables and the side bounds. The side bounds were determined based on two  $2^k$  factorial designs conducted with: lower and upper bounds of 1/128 and 1/2 of an inch, and 1/64 and 1/4 of an inch. The first design with the larger range demonstrated the the FEA simulation has stability issues when large difference of design variables exist. 29 of the 129  $2^k$  simulations failed to converge. In the second, smaller range design only a single  $2^k$  simulation failed to converge. Therefore, the second  $2^k$  factorial's upper and lower bounds were selected for the side bounds on the design variables.

Table 1: Constraints and Side bounds for optimization problem statement.

Constraints and Side bounds	
$f_{min}$	9.5 Hz
$\sigma_1$	60 ksi
$T_{max}$	1000 °F
$U_{max}$	0.10 inches
$X_{LB}$	1/64 inches
$X_{UB}$	1/4 inches

Utilizing the side bounds of the design variables, a LHS design was conducted with 200 design points. From this design exploration it was determined for temperatures under 1000 °F, the stresses and displacements were not critical. This is because the majority of the stress is caused by thermal expansion. Therefore, the stress constraint and the displacement constraint are removed. The resulting normalized optimization statement is as follows:

$$\begin{aligned}
 \text{Minimize:} \quad & f(\mathbf{x}) = \text{mass} \\
 \text{Subject to:} \quad & g_1(\mathbf{x}) = f/f_{min} - 1 \geq 0 \\
 & g_j(\mathbf{x}) = 1 - T_j/T_{max} \geq 0 \\
 \text{Design variables:} \quad & \mathbf{x} = [x_1, x_2, x_3, x_4, x_5, x_6, x_7]^T \\
 \text{Side bounds:} \quad & x_{LB} \leq x_i \leq x_{UB}
 \end{aligned} \tag{3}$$

This change in the optimization statement does not effect the difficulty of the problem, the frequency constraint will cause the panel to become thinner while the temperature constraint causes the panel to become thicker. Therefore, optimization is still being performed on competing constraints. The P-norm value from Equation 2 was selected to be 15.54 based on Fig. 12. A P-norm of 15.54 results in anywhere from 20 to 60 percent error. For temperature the error is around 20 to 30 percent. To account for this in the optimization routine the  $T_{max}$  is increased to 1300 °F and plus or minus 50°F is acceptable.

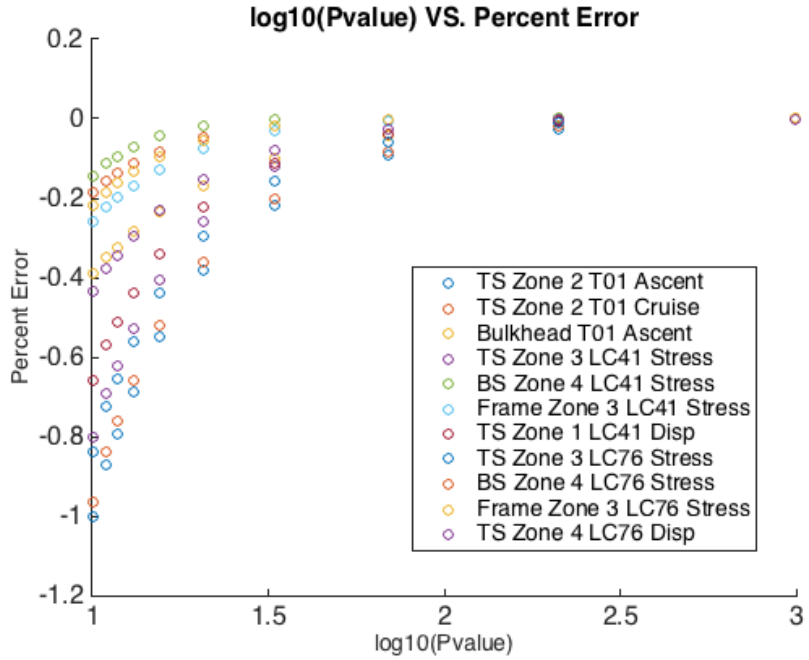


Figure 12: Percent error of the aggregated value from the true maximum per region as a function of P-norm.

The final optimization statement with the values for the bounds substituted is represented in Eq. 4. The final step before performing optimization is selecting an appropriate step size for finite difference. Therefore, a finite difference convergence study was performed with respect to each response. All 7 of the design variables were changed from 10 to .1 percent to determine the appropriate step size. The results for  $X_1$  are in Figures 21 through 23. The results for the other 6 variables are in Appendix 1.

$$\begin{aligned}
 \text{Minimize:} \quad & f(\mathbf{x}) = \text{mass} \\
 \text{Subject to:} \quad & g_1(\mathbf{x}) = f/9.5 - 1 \geq 0 \\
 & g_j(\mathbf{x}) = 1 - T_j/1300 \geq 0 \\
 \text{Design variables:} \quad & \mathbf{x} = [x_1, x_2, x_3, x_4, x_5, x_6, x_7]^T \\
 \text{Side bounds:} \quad & 1/64 \leq x_i \leq 1/4
 \end{aligned} \tag{4}$$

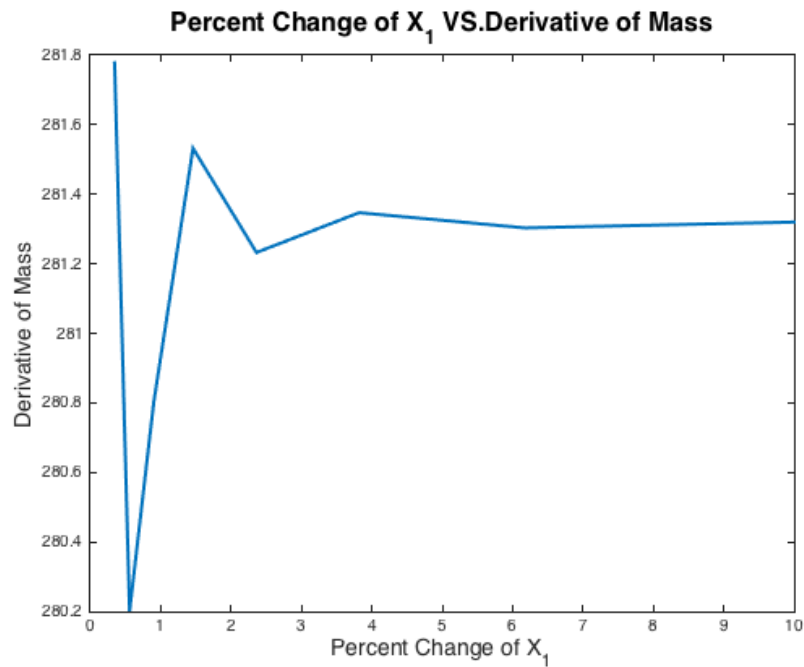


Figure 13: Finite difference convergence for  $X_1$  w.r.t. mass.

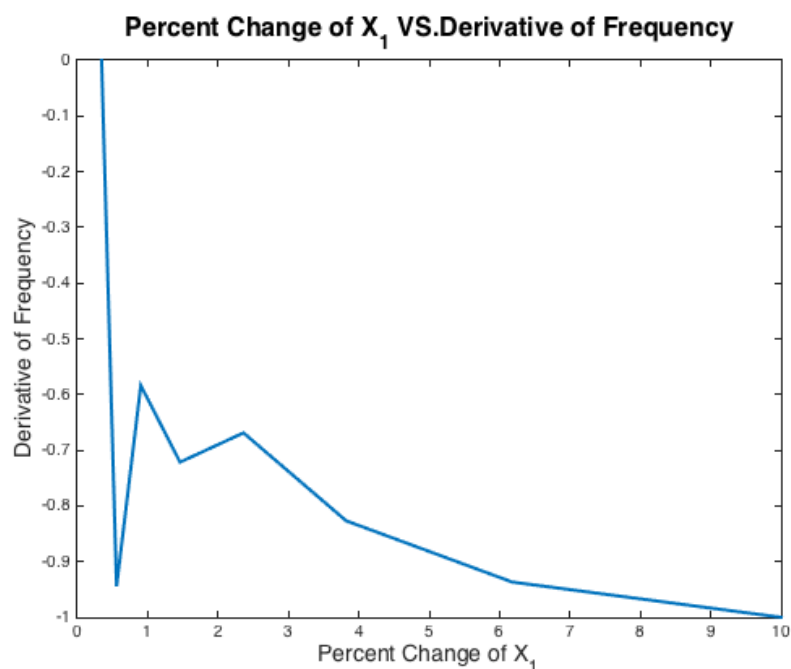


Figure 14: Finite difference convergence for  $X_1$  w.r.t. normalized frequency.

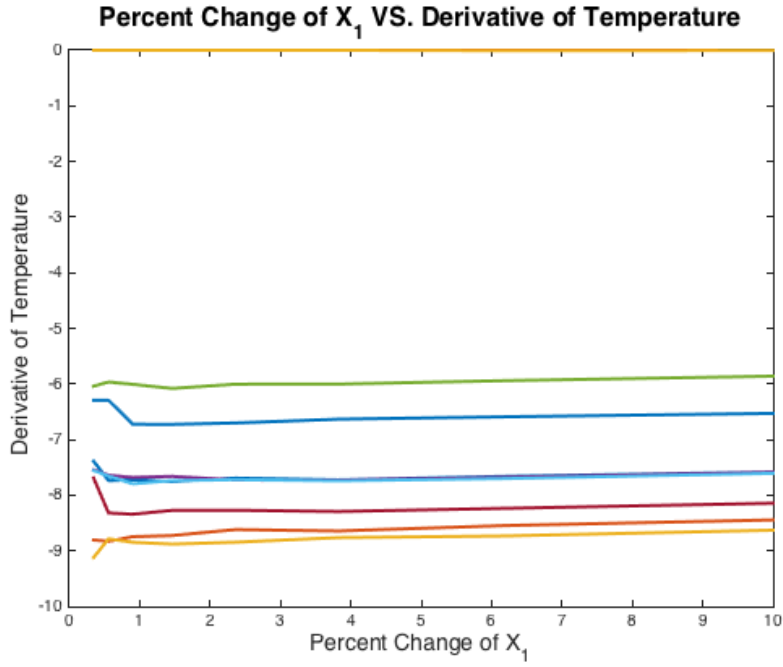


Figure 15: Finite difference convergence for  $X_1$  w.r.t. normalized temperature.

From the previous 3 figures and the results in Appendix 1, the step sizes were selected to be: a 5 percent change in all 7 variables for mass and frequency, and a 2.5 percent change for all 7 variables for all temperatures.

## DISCUSSION OF RESULTS

To perform the optimization an initial point was selected by creating a surrogate on the 200 LHS design points, and optimizing on the surrogate. However, when this analysis was performed the error between the surrogate and the FEA solution was drastic, implying that the surrogate has a low accuracy in the 7 dimensional space with only 200 points. Therefore, the LHS design point with the most feasible solution was utilized as the initial starting point for the gradient based optimization procedures. The initial design array in Table 2 is used for both interior point and the sequential function approximation techniques. The associated objective value and non-normalized constraints are in Table 3.

Table 2: Initial design variable array used for both interior point and sequential function approximation methods.

$x_1$	$x_2$	$x_3$	$x_4$	$x_5$	$x_6$	$x_7$
0.1736	0.2234	0.0704	0.1758	0.0878	0.1838	0.2272

Table 3: Initial objective value and non-normalized constraints used in both interior point and sequential function approximation methods.

Simulation	Response	Location	Quantity	Max	Max CAE	Error
FREQ	mass	Global	206.2344	—	—	—
	f	Global	12.269	—	—	—
T01	TS-Temp Ascent	Zone 1	1259.26878	1265.43133	778.700	62.51%
		Zone 2	1259.42159			
		Zone 3	1265.43133			
		Zone 4	1237.05679			
	TS-Temp Cruise	Zone 1	1250.66174			
		Zone 2	1249.88245			
		Zone 3	1255.24427			
		Zone 4	1227.18302			
	Bulkhead Ascent	Middle	929.214806			
	Bulkhead Cruise	Middle	931.599056			

Table 3 demonstrates that the P-norm selected can generate results that are more conservative than necessary, however to ensure differentiability the P-norm of 15.54 will be used through out the remainder of this paper.

### INTERIOR POINT ALGORITHM

The interior point algorithm is implemented via MATLAB's fmincon optimization function. Its objective is to decrease the objective value while maintaining a interior or feasible point within the design domain. Figure 16 depicts the objective value as a function of iteration history. Its easy to see that the objective value is consistently decreasing, unfortunately, in Fig. 17 it is notable that the interior point algorithm failed to maintain feasible while decreasing the objective value. The algorithm converged to an infeasible point.

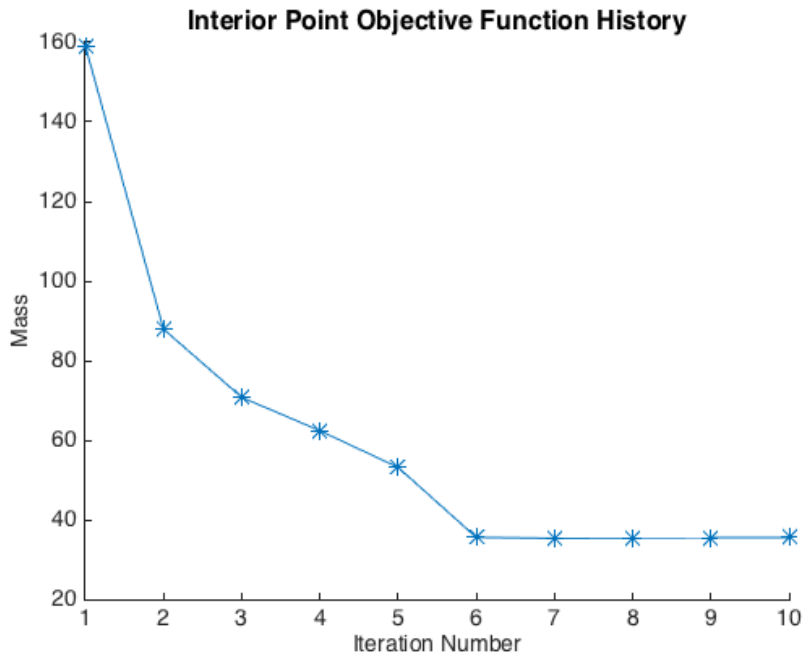


Figure 16: \*

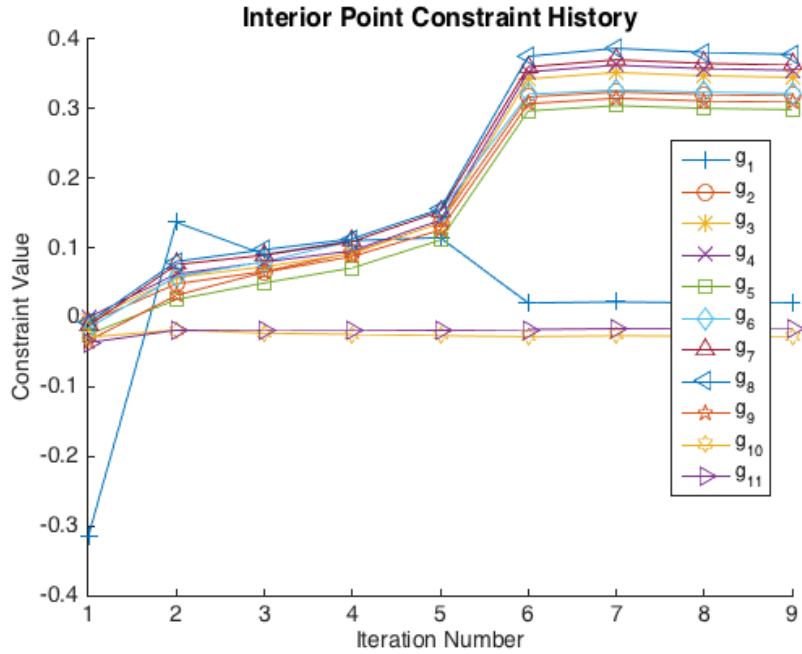


Figure 17: \*

It is notable that not every algorithm works for every problem, however it is likely that given a different initial point the algorithm may have converged.

### SEQUENTIAL FUNCTION APPROXIMATION

Sequential function approximations are used in a situation where the objective is to reduce the objective while maintaining feasibility. The result of this algorithm cannot be determined as optimal because the KKT conditions are never checked, however in most industries it is necessary to have an optimal design, only a better one than the original. The sequential function approximations is implemented with a convergence criteria of a change in mass less than 1 percent. The function approximation built at each FEA is the one point conservative approximation and MATLAB's interior point algorithm is used to optimize on the sub problem. The bounds for the side problem start out as 50 percent of the design domain and reduce by 10 percent after each FEA call. The Objective history is found in Fig. 18.

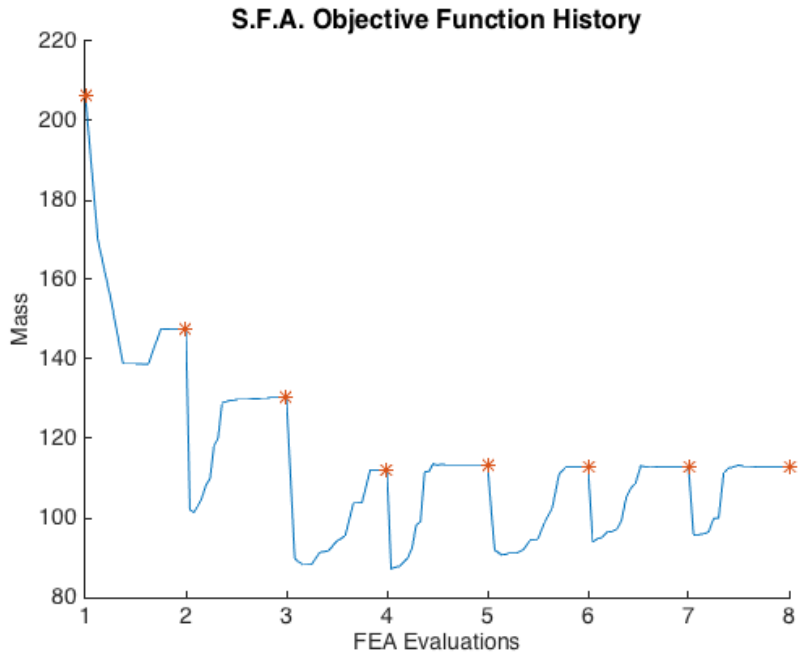


Figure 18: Objective history of the sequential function approximation method.

From the figure above, there are a series of notable spikes in objective history after each FEA evaluation. The spikes represent the iteration history of each individual sub problem call. The constraint history of the S.F.A. method and the design variable history are in Figures 19 and 20 respectively.

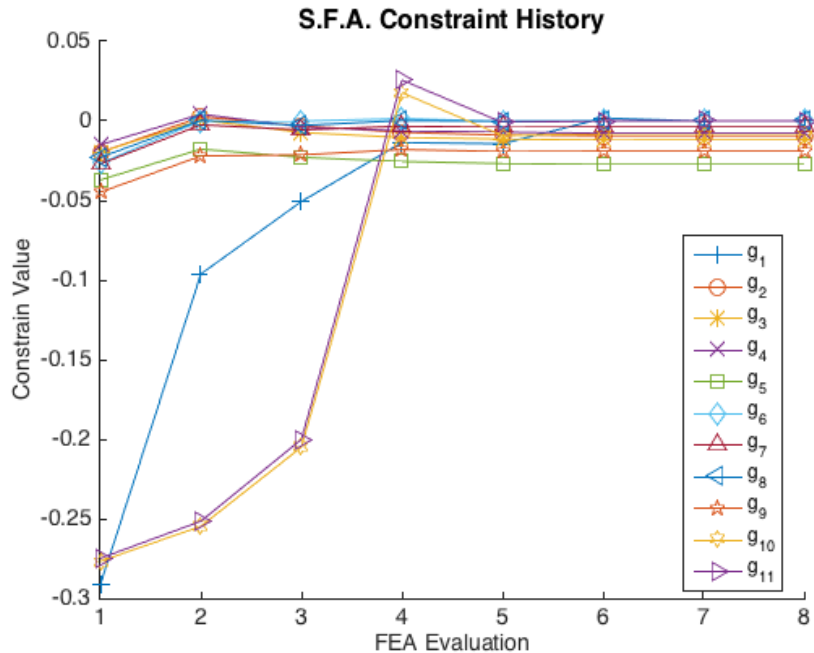


Figure 19: Constraint history of the sequential function approximation method.

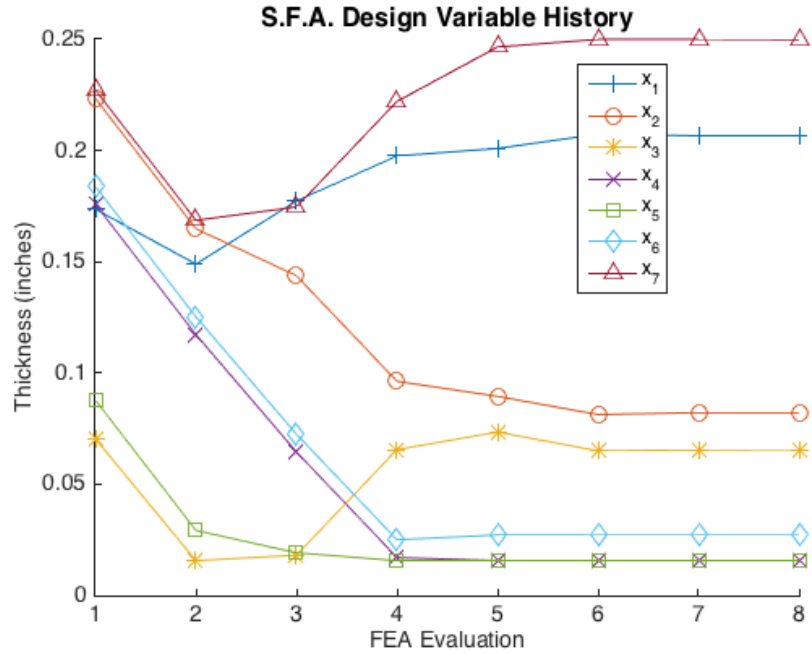


Figure 20: Design variable history of the sequential function approximation method.

## SUMMARY AND RECOMMENDATIONS

In summary, the optimized panel has a mass of 112.84 lbm, a natural frequency of 9.5 and experience a maximum temperature of 786 degrees F. The detailed results are in Table 4 and followed by the final design values in Table 5. It is notable that the 60 percent error was maintained in the aggregated value resulting in the temperature constraint being highly conservative. However, the results indicate at 40 percent decrease in mass. An additional study can be undertaken to increase the maximum aggregated temperature to 1600 and check the optimal solution. This should result in a lighter design. In addition to the study improvements previously mentioned,

Table 4: Responses of the improved panel design.

Simulation	Response	Location	Quantity	Max	Max CAE	Error
FREQ	mass	Global	112.8426	—	—	—
	f	Global	9.5	—	—	—
T01	TS-Temp Ascent	Zone 1	1272.78369	1284.73008	1284.730	63.45%
		Zone 2	1269.31513			
		Zone 3	1274.80698			
		Zone 4	1249.68154			
	TS-Temp Cruise	Zone 1	1284.73008			
		Zone 2	1279.80841			
		Zone 3	1284.72959			
		Zone 4	1260.29401	1284.730	786.000	
	Bulkhead Ascent	Middle	1274.20856			
	Bulkhead Cruise	Middle	1284.70585			

it is believed that relaxing the constraint temperature to 1200 degrees, the aggregated value to 2000, and incorporating the stress back into the optimization problem could make an interesting study. However, the results of the study can be considered successful. The panels mass was

Table 5: Design values for the improved panel design

$x_1$	$x_2$	$x_3$	$x_4$	$x_5$	$x_6$	$x_7$
0.1736	0.2234	0.0704	0.1758	0.0878	0.1838	0.2272

successfully decreased by 40 percent and the resulting design is feasible and conservative.

## REFERENCES

- [1] Zuchowski, B., "Predictive Capability for Hypersonic Structural Response and Life Prediction, Phase 1–Identification of Knowledge Gaps," Tech. rep., Technical Report AFRL-RB-WP-TR-2010-3069, Air Force Research Laboratory, Lockheed Martin Corp, 2010.
- [2] Zuchowski, B., "Predictive Capability for Hypersonic Structural Response and Life Prediction, Phase 2–Detailed Design of Hypersonic Cruise Vehicle Hot-Structure," Tech. rep., Technical Report AFRL-RQ-WP-TR-2012-0280, Air Force Research Laboratory, Lockheed Martin Corp, 2012.

## APPENDIX 1: FINITE DIFFERENCE CONVERGENCE

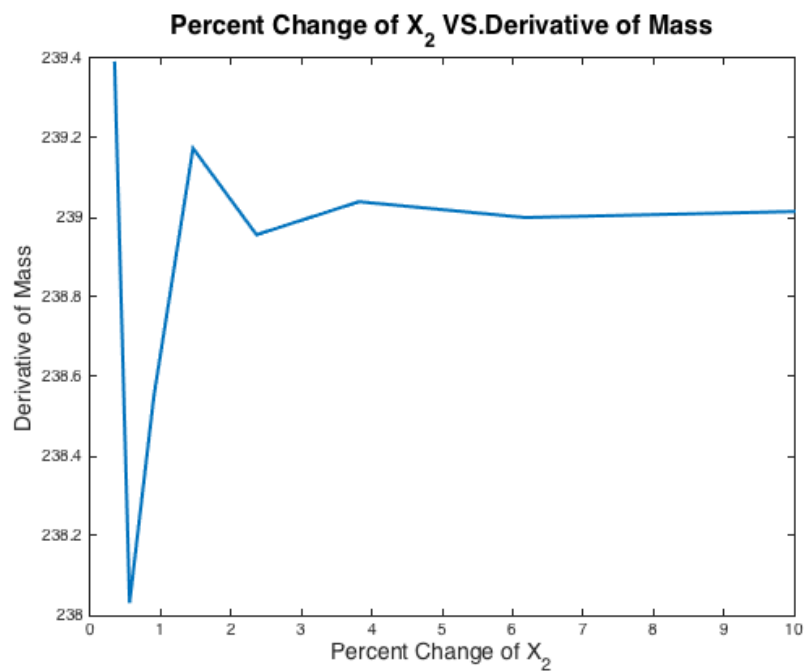


Figure 21: Finite difference convergence for  $X_2$  w.r.t. mass.

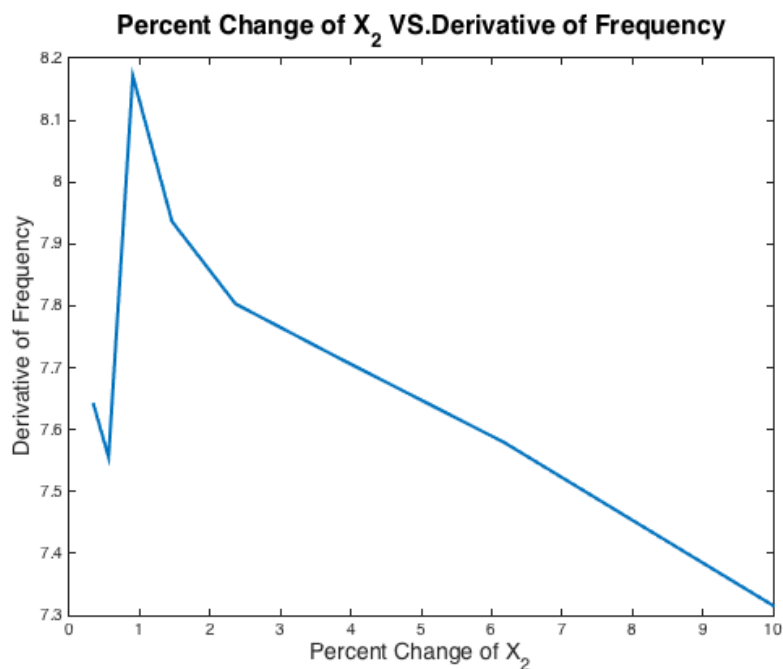


Figure 22: Finite difference convergence for  $X_2$  w.r.t. normalized frequency.

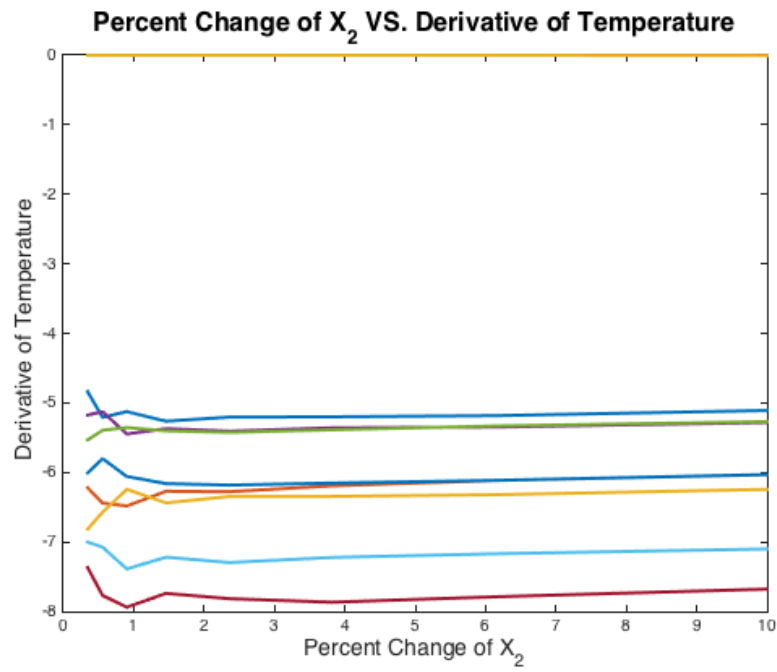


Figure 23: Finite difference convergence for  $X_2$  w.r.t. normalized temperature.

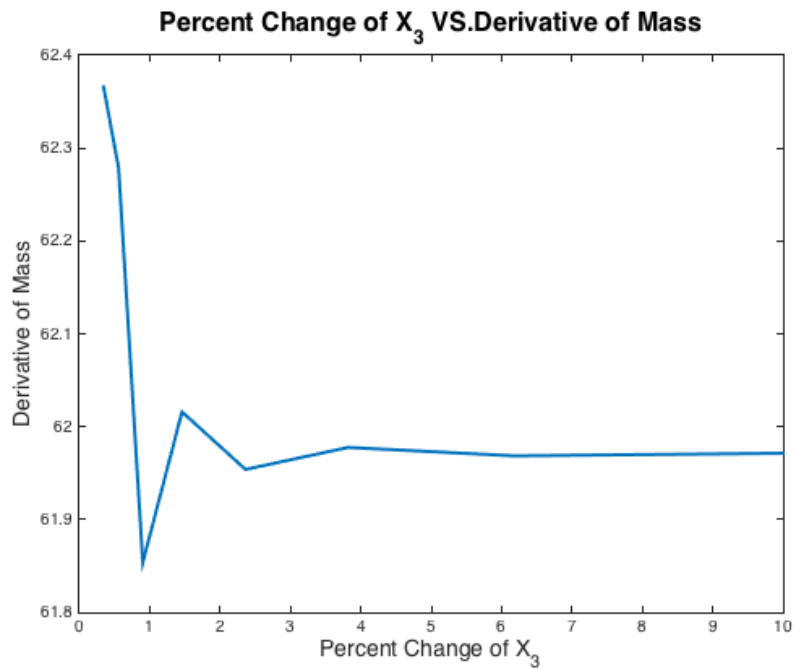


Figure 24: Finite difference convergence for  $X_3$  w.r.t. mass.

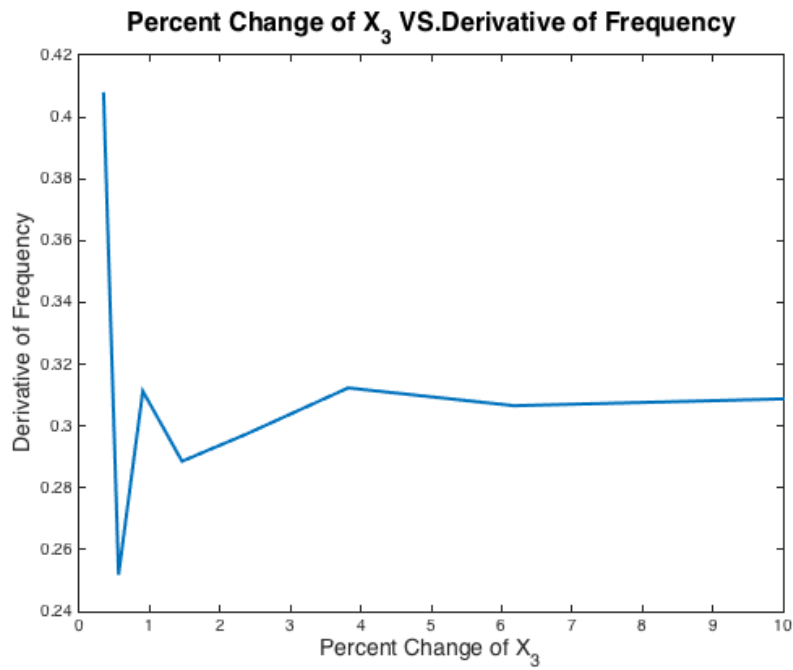


Figure 25: Finite difference convergence for  $X_3$  w.r.t. normalized frequency.

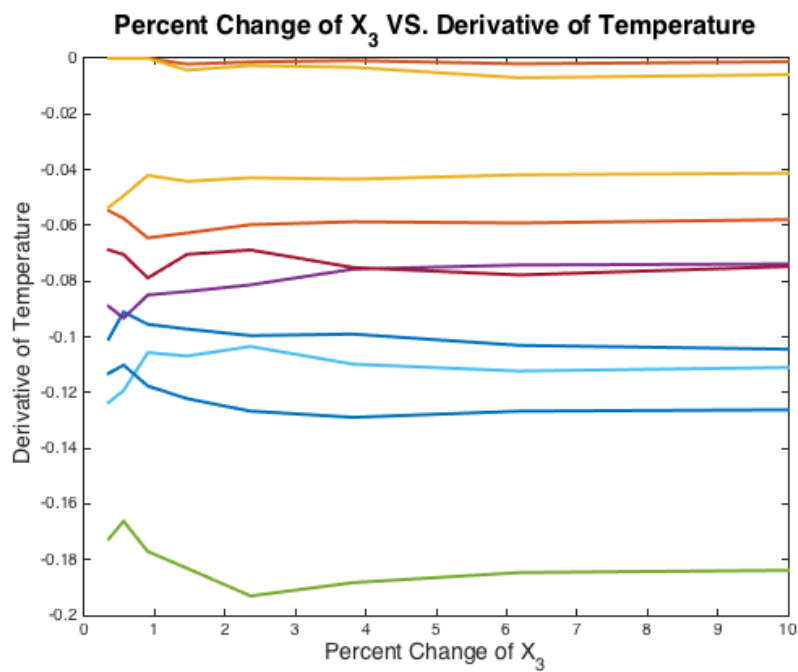


Figure 26: Finite difference convergence for  $X_3$  w.r.t. normalized temperature.

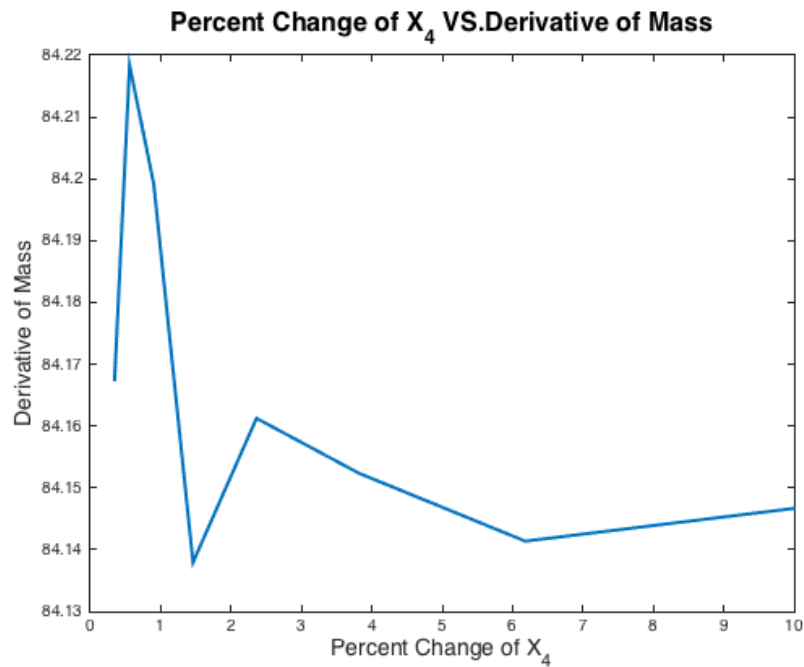


Figure 27: Finite difference convergence for  $X_4$  w.r.t. mass.

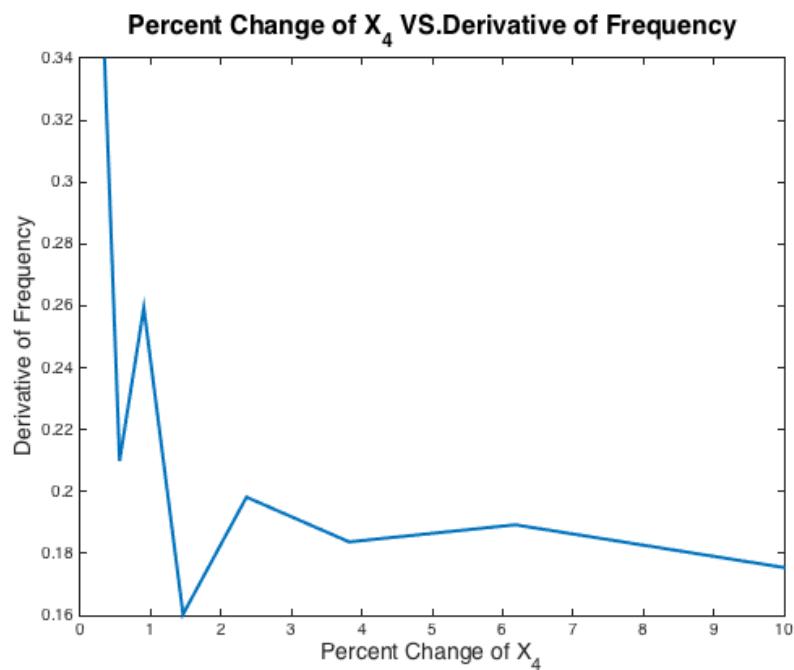


Figure 28: Finite difference convergence for  $X_4$  w.r.t. normalized frequency.

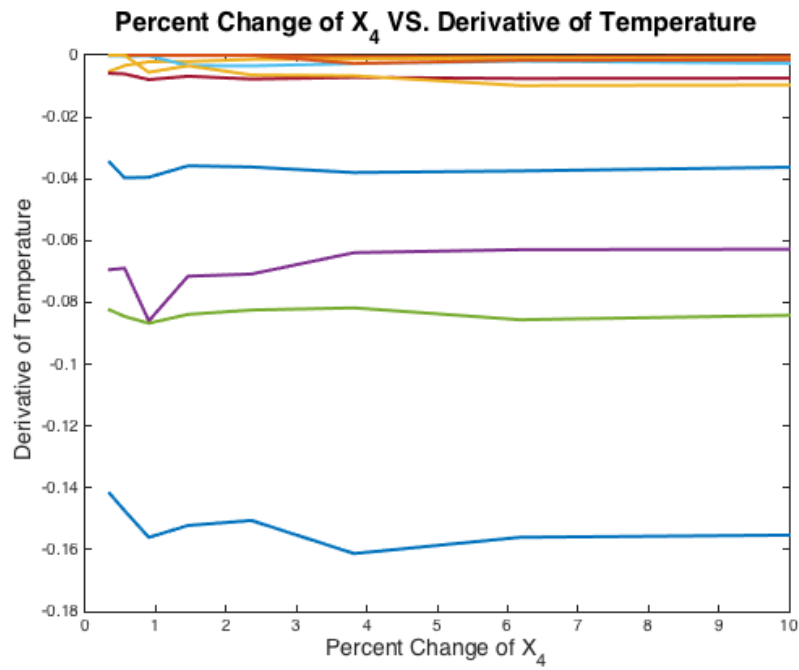


Figure 29: Finite difference convergence for  $X_4$  w.r.t. normalized temperature.

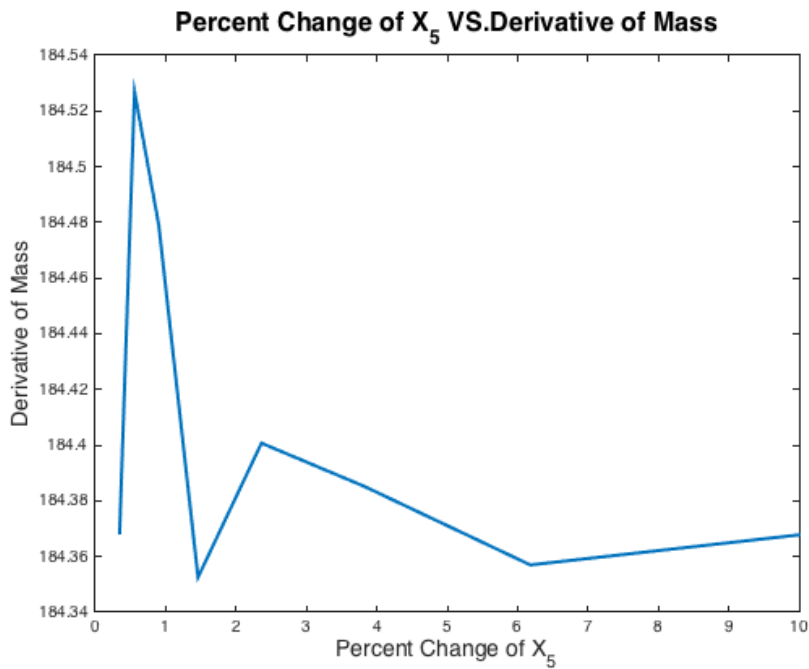


Figure 30: Finite difference convergence for  $X_5$  w.r.t. mass.

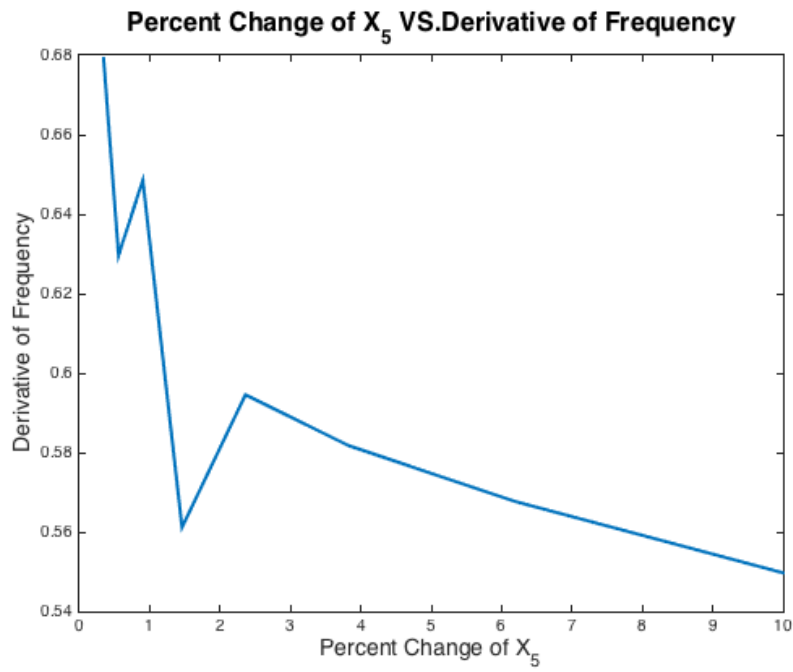


Figure 31: Finite difference convergence for  $X_5$  w.r.t. normalized frequency.

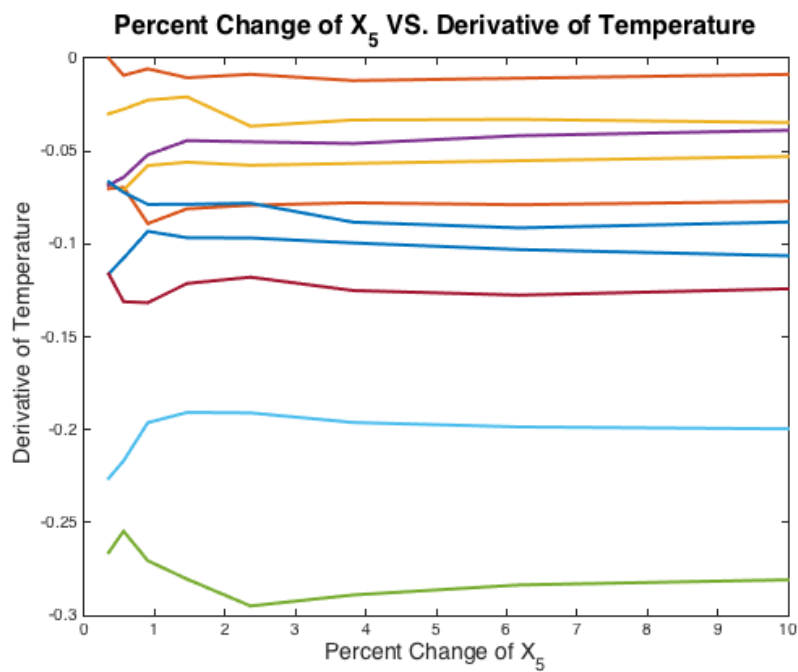


Figure 32: Finite difference convergence for  $X_5$  w.r.t. normalized temperature.

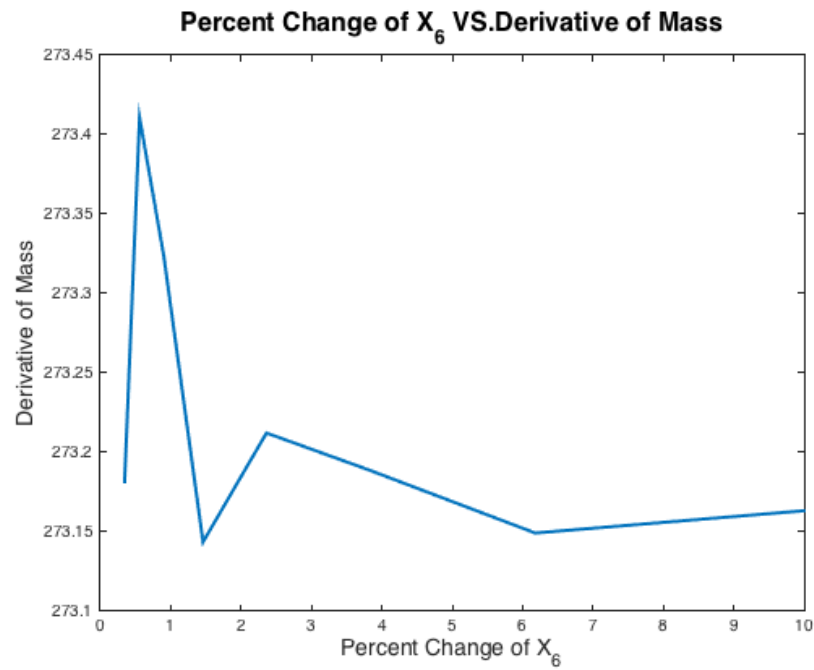


Figure 33: Finite difference convergence for  $X_6$  w.r.t. mass.

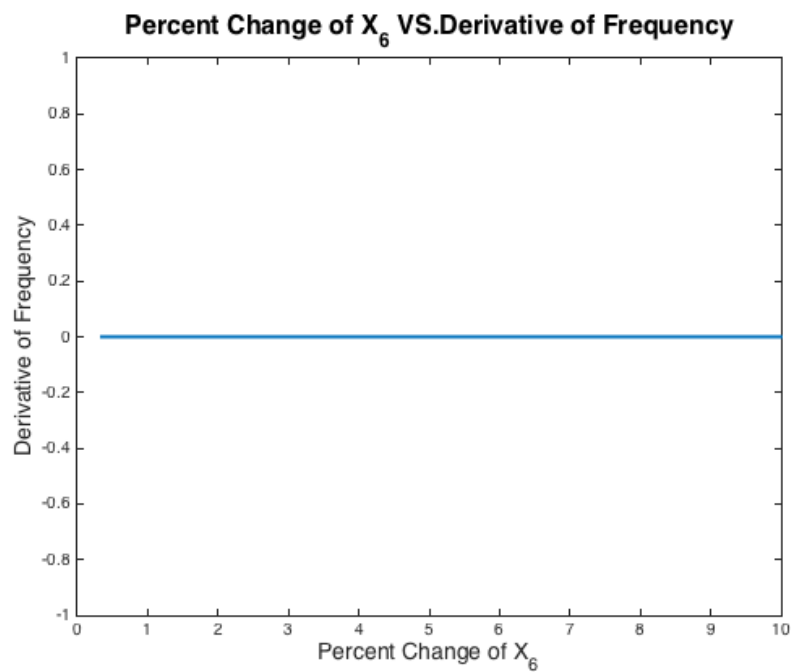


Figure 34: Finite difference convergence for  $X_6$  w.r.t. normalized frequency.

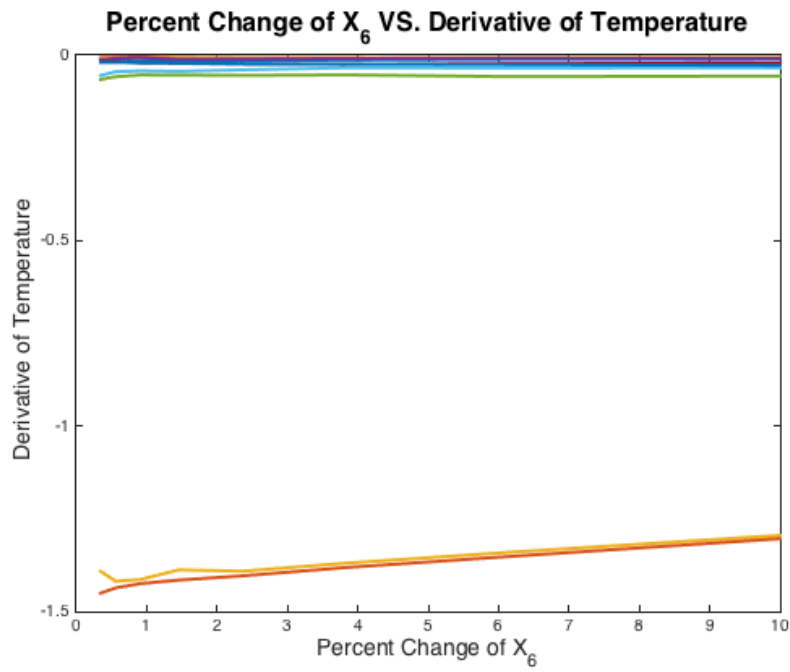


Figure 35: Finite difference convergence for  $X_6$  w.r.t. normalized temperature.

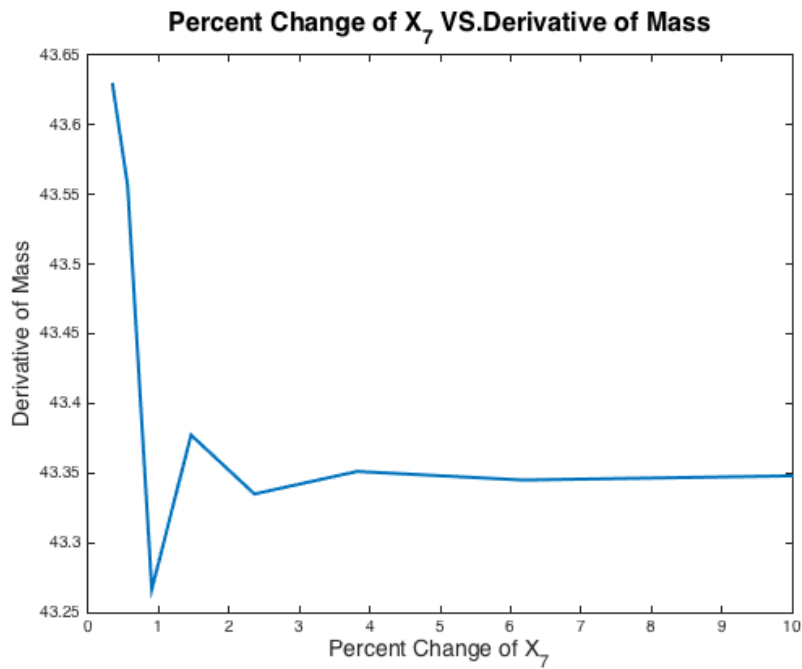


Figure 36: Finite difference convergence for  $X_7$  w.r.t. mass.

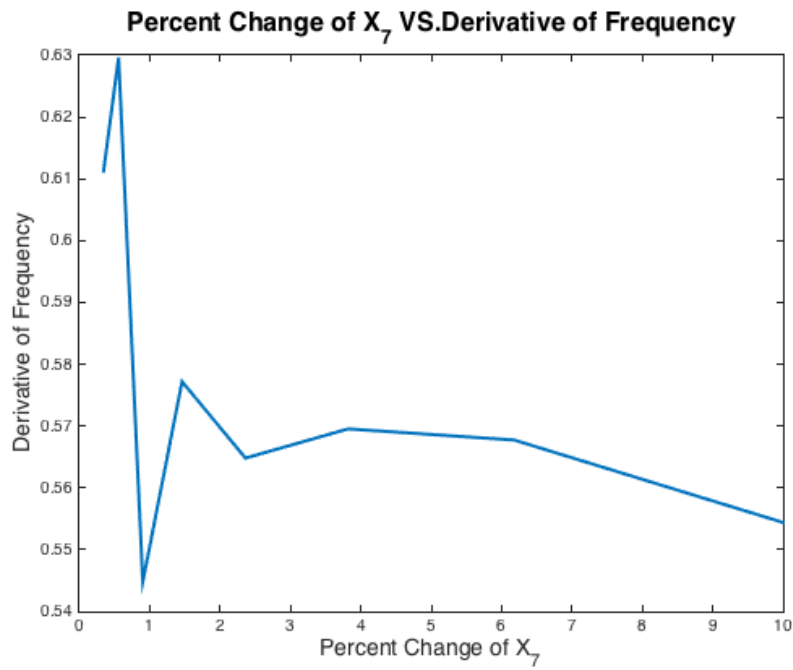


Figure 37: Finite difference convergence for  $X_7$  w.r.t. normalized frequency.

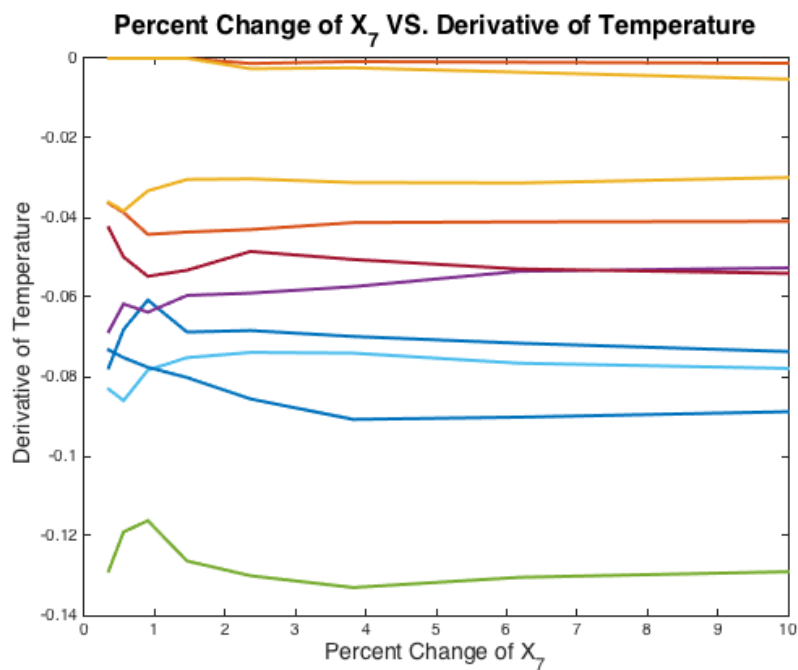


Figure 38: Finite difference convergence for  $X_7$  w.r.t. normalized temperature.

## APPENDIX 2: SAMPLE ANALYSIS

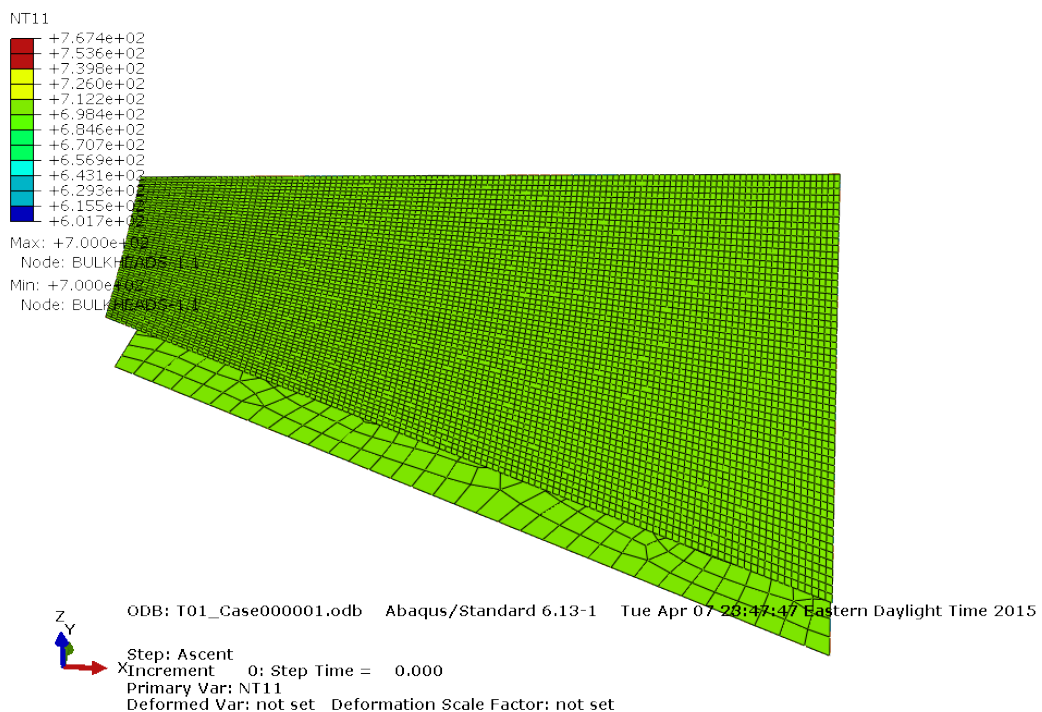


Figure 39: Initial Temperature of the top-skin and bottom bulkhead during the T01 analysis.

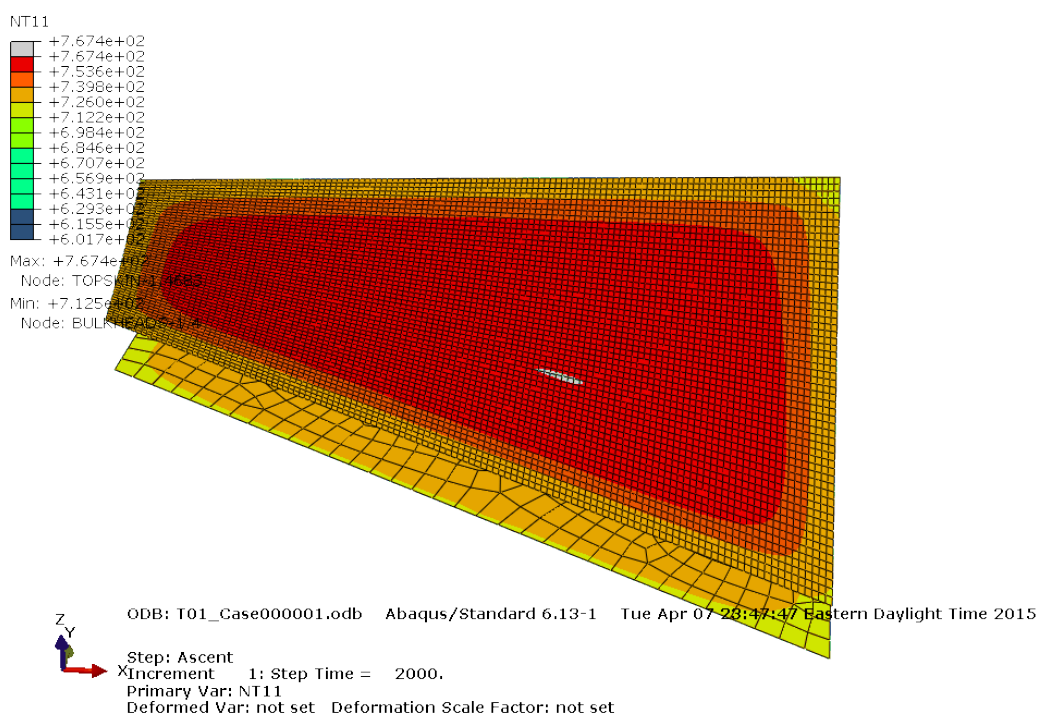


Figure 40: Ascent Temperature of the top-skin and bottom bulkhead during the T01 analysis.

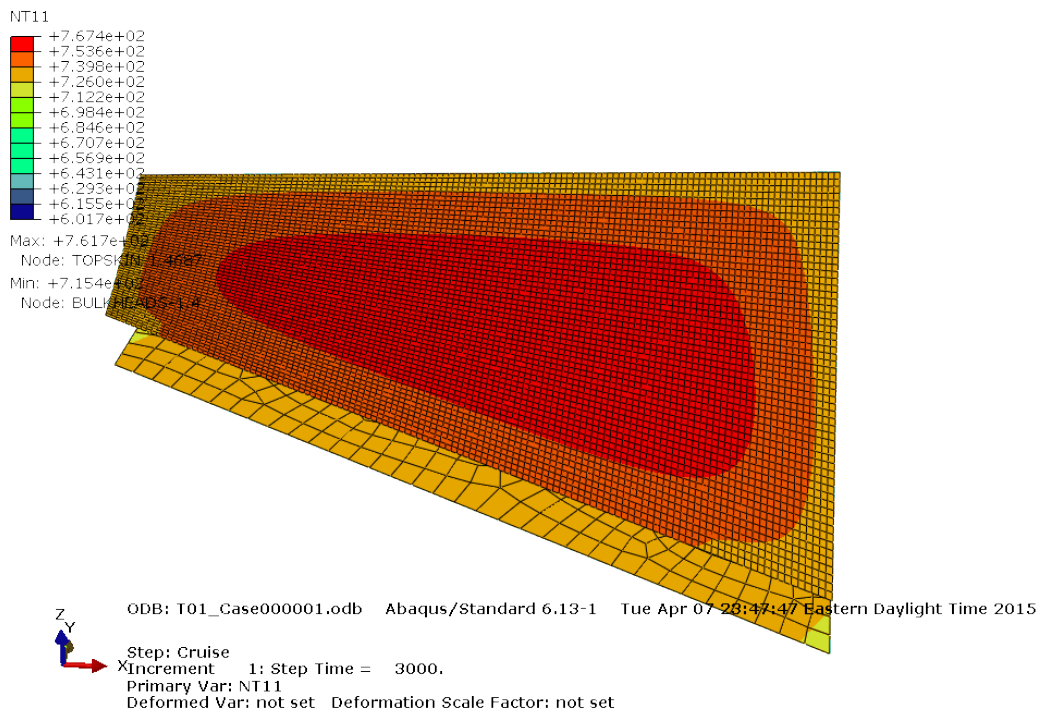


Figure 41: Cruise Temperature of the top-skin and bottom bulkhead during the T01 analysis.

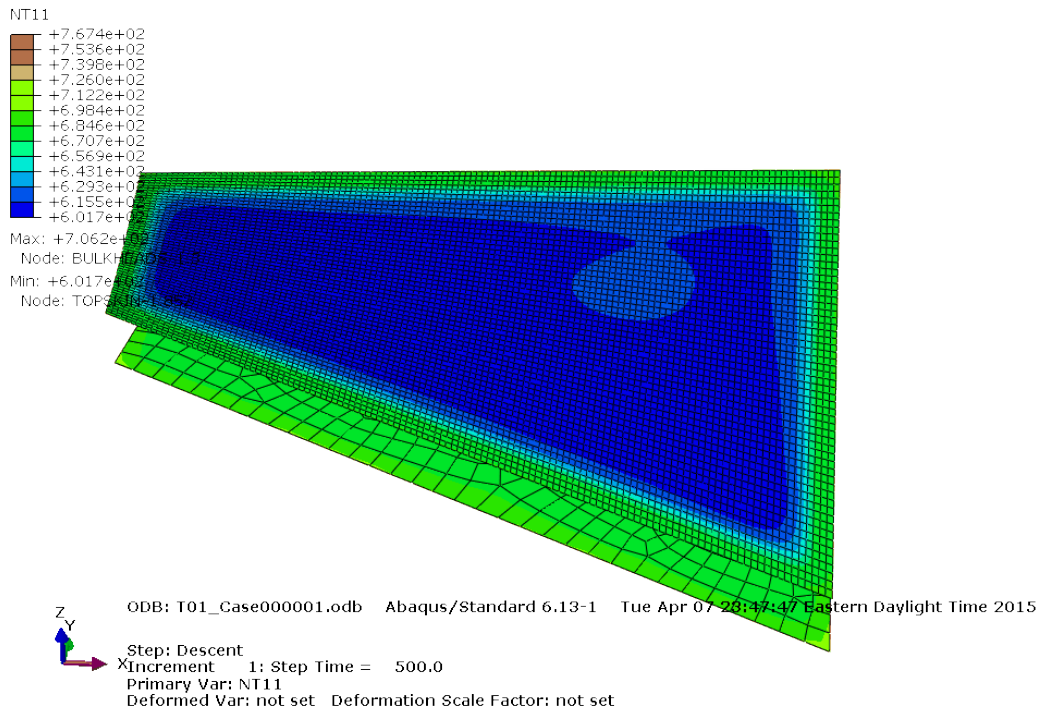


Figure 42: Descent Temperature of the top-skin and bottom bulkhead during the T01 analysis.

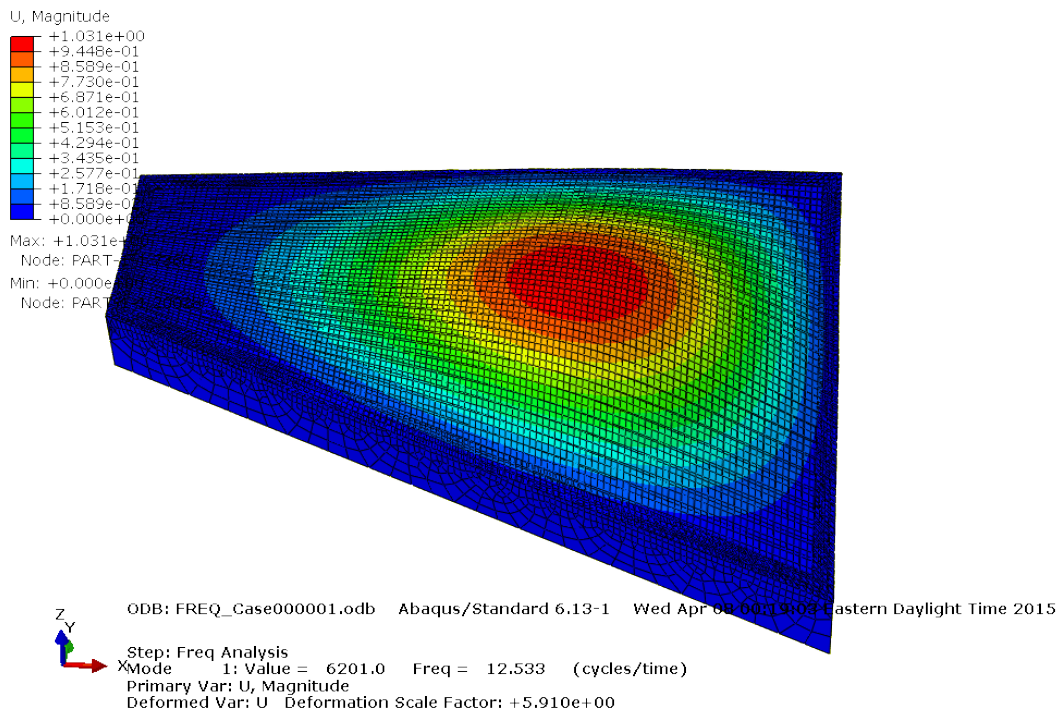


Figure 43: First mode shape of the entire assembly.

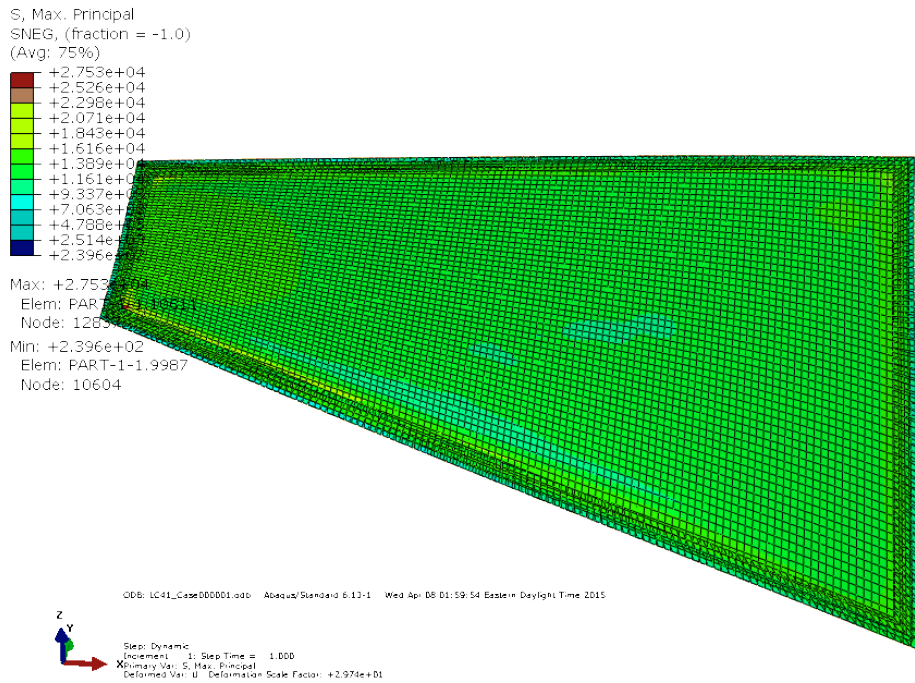


Figure 44: Stress of the top-skin, bottom-skin and frame during the LC41 analysis.

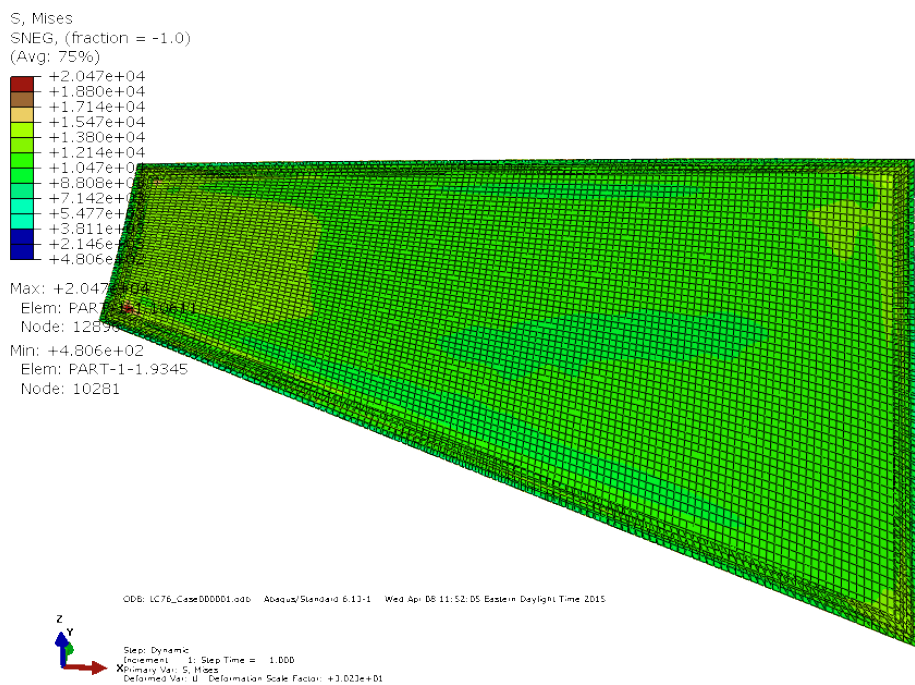


Figure 45: Stress of the top-skin, bottom-skin and frame during the LC76 analysis.